NUMERICAL AND EXPERIMENTAL INVESTIGATION OF SHAPE MEMORY ALLOYS SUBJECT TO COMPLEX MECHANICAL LOADING: A CASE STUDY OF A NITI HELICAL SPRING

Miroslav Frost[⋆], Petr Sedlák[⋆], Lukáš Kadeřávek[†], Luděk Heller[†]

[⋆]Institute of Thermomechanics, Czech Academy of Sciences
Dolejškova 5, Prague, 18200, Czech Republic
mfrost@it.cas.cz

[†]Institute of Physics, Czech Academy of Sciences
Na Slovance 2, Prague, 18221, Czech Republic

Keywords: Shape memory alloys, Helical spring, Complex loading, Simulations, Experimental validation.

Summary: *Shape memory alloys (SMA) are metallic materials exhibiting unusual properties of being able to sustain and recover large strains (superelasticity) and to "remember" the initial configuration and return to it with temperature change (one-way shape memory effect). These properties make them very suitable for utilization as actuators. One of the simplest possible geometry in terms of manufacturing and utilization is the form of a helical spring. For its optimal design and control detailed information on evolution of internal state of the material during operation is advantageous. In this work a macroscopic constitutive model tailored for NiTi shape memory alloys exhibiting R-phase transition, transformation strain anisotropy and tension-compression asymmetry is employed. It features an elaborated, asymmetric form of the rate independent dissipation function coupling martensitic transformation and reorientation processes, whose specific form was inspired by experimental observations. Numerical simulations of mechanical loading of the spring at various temperatures compared with macroscopic experimental data confirm good predictive capability of the model. Because of naturally non-proportional loading mode combining bending and torsion, distributions of stress components within cross-section of the wire predicted by the model are quite complex. They allow to identify potential loci of initiation of irreversible deformation for this type of loading.*

1. INTRODUCTION

Due to amazing effects linked to martensitic phase transformation and subsequent evolution of microstructure, shape memory alloys (SMA) are classified under smart materials attractive for utilization in actuator applications. The form of a helical spring may provide advantages of light weight, large recoverable deformation, high energy density and manufacturing simplicity. However, even in such an "unsophisticated design", the material is deformed in a complex, non-proportional way when the spring is simply stretched.

As demonstrated in [1], the macroscopic mechanical response of SMA is very sensitive to variation of loading conditions when multiple deformation mechanisms are active. Following experimentally observed phenomena influence the mechanical response of SMA: joint influence of stress and temperature on phase transitions, interaction of phase transformation and reorientation processes, different elastic properties of phases, elastic properties of martensite depending on the loading mode (different for tension and for compression loading in particular) or tension-compression asymmetry and anisotropy of transformation strain. Things got even more complicated when the transformation proceeds via intermediate phase as in the case of R-phase in NiTi alloys.

Recently, several "macroscpic" (continuum mechanics) models tackling the issue of general thermomechanical loading of SMA have appeared in the literature. They cover processes occurring in the material at microscopic level by introduction of internal variables, which extend description of thermodynamic state in a material point. Particularly, internal variables allow to capture dissipation connected to the these processes by prescribing either limit ("yield") functions [2–7] or, equivalently, a dissipation function [8–10]. Often, reliability and robustness of numerical implementation of the constitutive models is tested on benchmark simulations of a helical spring [5, 8, 10–16]. Naturally, usually presented total macroscopic response in terms of force-stroke (load-deflection) dependence provides reasonable global estimate of actuator's performance. Nevertheless, very similar macroscopic "curves" may result from quite different microscopic state of the material in the spring and detailed information of internal state of material may be still important for better temperature/actuation control or fatigue prevention [17].

In this study, the model [9] is employed to reproduce the macroscopic response and to examine the stress state of a helical NiTi spring subject to stretching. Since the model features an elaborated form of dissipation function combining transformation and reorientation contributions, includes R-phase transition and material anisotropy, it is particularly suitable for simulations of a shape set NiTi wire springs. The results are compared to a series of dedicated experimental measurements on such springs. The macroscopic response in terms of force-stroke dependence at different temperatures is studied and interpreted with respect to information on internal state (stress components distributions) provided by the model.

2. EXPERIMENTAL

Helical springs were shape set from superelastic 0.2 mm thin NiTi wires (FWM NiTi#1-SE) using an in-house designed and built stainless steel fixtures in a cylindrical salt bath furnace at 510 °C for 10 min. A micrograph of a typified 2.6-coil helical spring with initial outer diameter 3.2 mm and initial height 3.9 mm is presented in Fig. 1. Mechanical testing was performed with an in-house assembled testing device featuring a linear actuator (maximum speed 100 mm/s) and a sensitive load cell (maximum load 10 N). The maximum stroke was 20 mm corresponding to reduction of the spring diameter by approx. 80%. To ensure isothermal conditions and good heat transfer at each test, experiments were conducted in a temperature-controlled, thermally insulated Peltier air furnace with airtight-sealed sample inlets at very slow loading rate (1.5 mm/min). Force, stroke and temperature data were recorded continuously.
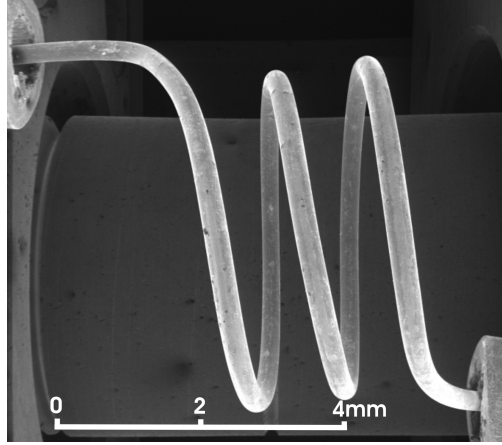
Figure 1. A micrograph of a typified helical spring used in experiments.

3. MODELLING

The dimensions of spring listed in the previous section were used in simulations. The relatively high spring index, $D_0 = 15$, allows for utilization of Euler beam approximation. However, because of large recoverable strains attainable in SMA, the spring could be repeatedly deformed up to more than 500% deflection. Hence, large deflection mode connected with substantial spring diameter reduction and large beam rotation must be considered. Let us also note that due to the high spring index, strains attained within the cross-section are relatively small even at the maximum deflection ($< 7\%$).

To simplify simulations, the boundary conditions enforced in real experiments were replaced by translational periodic boundary conditions corresponding to the infinite spring. The assumption that cross-sections remain planar and perpendicular to the longitudinal axis during deformation is well satisfied in our particular geometry. Distributions of examined physical quantities are thus homogeneous along the wire axis and the problem can be reduced to determination of their planar distribution within a single cross-section of the wire. Due to presumed strong dominance of torsion and bending, only two components of stress tensor (tensile/compressive and torsional) are considered in computations.

Since complex constitutive equations of SMA lead to non-trivial integration of the response through cross-section [14], numerical computation of the total response is needed. The cross-section of the wire is divided into a dense finite mesh with 780 integration points in total. Piecewise constant basis functions are used to determine the planar distribution of two-component stress and transformation strain, and volume fraction of martensite and R-phase. Spatially and temporally constant temperature is prescribed in all integration points.

The constitutive response is obtained utilizing rate-independent continuum-based model capturing occurrence of R-phase and transformation anisotropy based on the work [9]. The model introduces four internal variables (volume fraction of martensite, volume fraction of

3

Miroslav Frost, Petr Sedlák, Lukáš Kadeřávek and Luděk Heller

R-phase, transformation strain of martensite and transformation strain of R-phase) and it is assembled by definition of a particular form of energy function (thermodynamic potential) and dissipation function dependent on strain, temperature and internal variables of martensite. Since hysteresis (hence dissipation) of the R-phase transformation is very small compared to transformation to martensite, see e.g. [18, 19], macroscopic changes of material response related to R-phase can be effectively modelled through a hyperelastic (non-dissipative) approximation. Namely, the inelastic strain of R-phase appears in the elastic part of the free energy and the chemical part is extended by an additional term depending on the volume fraction of R-phase. Hence, maximum transformation strain of R-phase, equilibrium temperature of austenite-R-phase transformation and related entropy difference are additional material parameters of the model. A restriction of maximum transformation strain tensor based on its invariants is imposed through a specific material function so that volume preserving property, tension-compression asymmetry and (texture-induced) transformation strain anisotropy observed in experiments are respected by the model. Furthermore, a particular form of phase- and transformation strain-

Parameter	Value	Unit	Brief description
$E^{\mathrm{A}}, E^{\mathrm{M},0}$	$71, 50$	[GPa]	Young moduli of austenite and thermally induced martensite.
$G^{\mathrm{A}}, G^{\mathrm{M},0}$	$25, 17$	[GPa]	Shear moduli of austenite and thermally induced martensite.
k, k^{R}	$0.06, 0.008$	[1]	Maximum transformation strain of martensite and R-phase in tension.
a	0.98	[1]	Tension-compression asymmetry parameter.
α^{A}	$1.1 \cdot 10^{-5}$	[1/°C]	Coefficient of thermal expansion of austenite.
$A, B, \varphi, \ldots$	$1, 1, 0$	[1]	Parameters of anisotropic transform. strain surface
$\ldots, L, M, N$	$1, 1.44, 1.44$	[1]	if the wire axis aligned with the x-direction, see [9].
$A_{\mathrm{s}}, A_{\mathrm{f}}$	$-1, 4$	[°C]	Temperature parameters related to the direct phase
$M_{\mathrm{s}}, M_{\mathrm{f}}$	$-1, -4$	[°C]	transformation between austenite and martensite,
T_0	-1	[°C]	see [9] for details.
$R_{\mathrm{s}}, R_{\mathrm{f}}$	$35, 20$	[°C]	Temperature parameters related to the R-phase transformation.
σ_0^{reo}	95	[MPa]	Martensite reorientation stress at T_0.
Σ^{reo}	-0.9	[MPa/°C]	Change of reorientation stress with temperature.
$\Delta s^{\mathrm{AR}}, \Delta s^{\mathrm{AM}}$	$0.121, 0.364$	[MPa/°C]	Difference between specific entropy of martensite-austenite and R-phase-austenite transformations.
$E^{\mathrm{int}}, E^{\mathrm{int,R}}, c^{\mathrm{reg}}$	$60, 80, 0.01$	[MPa]	Parameters of regularization function r, see [9].

Table 1. The set of material parameters used in simulations.

4

dependent tensor of elastic constants allows to capture substantially different elastic properties of austenite, temperature-induced martensite and (generally anisotropic) stress-induced martensite.

The mechanical response in a material point is then determined through so-called principle of minimum dissipation potential. More detailed introduction of the model including physical motivation, description of material parameters and numerical implementation can be found in [9, 12, 20].

Material parameters of the wire used in the constitutive model are summarized in Tab. 1. The elastic tensors describing elasticity of martensite "fully reoriented" in tension/compression take the particular form (Voight notation, GPa unit):

$$
\mathbb{C}_x^{\mathrm{M,t}} =
\begin{bmatrix}
192 & 152 & 152 & 0 & 0 & 0 \\
 & 182 & 125 & 0 & 0 & 0 \\
 & & 182 & 0 & 0 & 0 \\
 & & & 28.5 & 0 & 0 \\
 & \mathrm{symm} & & & 22.3 & 0 \\
 & & & & & 22.3
\end{bmatrix},
\mathbb{C}_x^{\mathrm{M,c}} =
\begin{bmatrix}
182 & 125 & 125 & 0 & 0 & 0 \\
 & 192 & 165 & 0 & 0 & 0 \\
 & & 192 & 0 & 0 & 0 \\
 & & & 13.5 & 0 & 0 \\
 & \mathrm{symm} & & & 22.3 & 0 \\
 & & & & & 22.3
\end{bmatrix},
$$

for axis of tension/compression in the x-direction.

4. RESULTS

To demonstrate capabilities of our modelling approach, a uniaxial superelastic response in a single material point predicted by the model is compared with experimental data reported in [21] in Fig. 2. Except for higher transformation strain ($k = 0.07$), material parameters presented in Tab. 1 were used. The model fits the experimental data very well except for martensitic transformation (pseudo-)hardening at compression, which is somehow underestimated by the model. Because of tension-compression asymmetry of transformation strain, the transition to martensite starts at higher stress and the transformation plateau is shorter in compression than in tension, and the total dissipated energy is lower. Different Young moduli of austenite, martensite in tension and martensite in compression are easily distinguishable both in experiments and simulations. The influence of R-phase is also worth noting; the transformation from austenite to R-phase is clearly visible in the initial stage of tension (different apparent Young moduli) but not in compression. This is attributed to the coupled effect of stress and temperature on the initiation of the transformation (the Clausius-Clapeyron-type of relation): since the transformation strain of R-phase in compression is lower than in tension, the transformation to R-phase would initiate at higher stress (at the same temperature), but it is effectively suppressed by the direct transformation to martensite.

Fig. 3a)–e) shows comparison of experimental and simulated force-stroke responses of the helical spring at constant temperatures of -10, 0, 20, 40 and 60 °C. They feature hysteresis with a long "plateau" (steeper at higher temperatures) and increasing force required to reach the maximum stroke with increasing temperature. As expected, this is due to phase transformations in the material. The spring exhibits remanent deformation after full unloading at the lowest

temperature ($-10\,^{\circ}$C) and the original length is recovered by heating (not shown) – as confirmed by the simulation. At $0\,^{\circ}$C, the "S-shaped" initial part of loading curve corresponds to continuous increase of transformation strain of R-phase followed by transformation to martensite. The spring returns to the initial length after unloading. At positive temperatures, the fully reversible evolution up to $\sim$5 mm stroke reflects transformation between austenite and R-phase. The effective modulus there increases with temperature, which is given by the steep Clausius-Clapeyron slope (d$\boldsymbol{\sigma}$/dT) of R-phase triggering [18]. With increasing temperature, the total area under hysteresis loop decreases, which is also well reproduced by the model.

Contour plots of distribution of two dominant components of stress – out-of-plane tensile/compressive stress and in-plane shear stress – within the wire cross-section are presented in Fig. 3f). They were generated by the model for loading at 16 mm stroke and temperatures -10, 20 and 60 $^{\circ}$C (see black circles in Fig. 3a), c), e)) and the leftmost point of each plot corresponds to the closest point of the cross-section to the spring axis. Since attained force increases with temperature, the maximum stress within the cross-section also increases. However, even though the actual geometry of the spring is the same, stress-distributions differ qualitatively. The maximum of the tensile stress shifts from the leftmost part of the surface towards
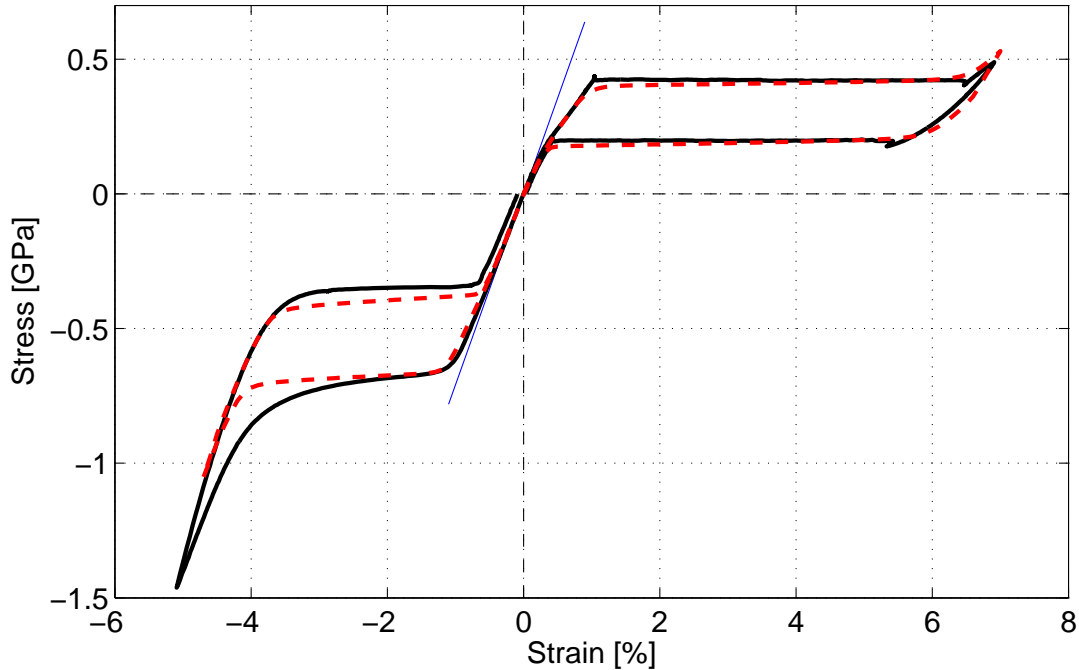

Figure 2. Simulation of uniaxial superelastic response of NiTi SMA (dashed red line) compared with data reported in [21] (solid black line). Thin blue line shows extrapolation of elastic response of pure austenite.
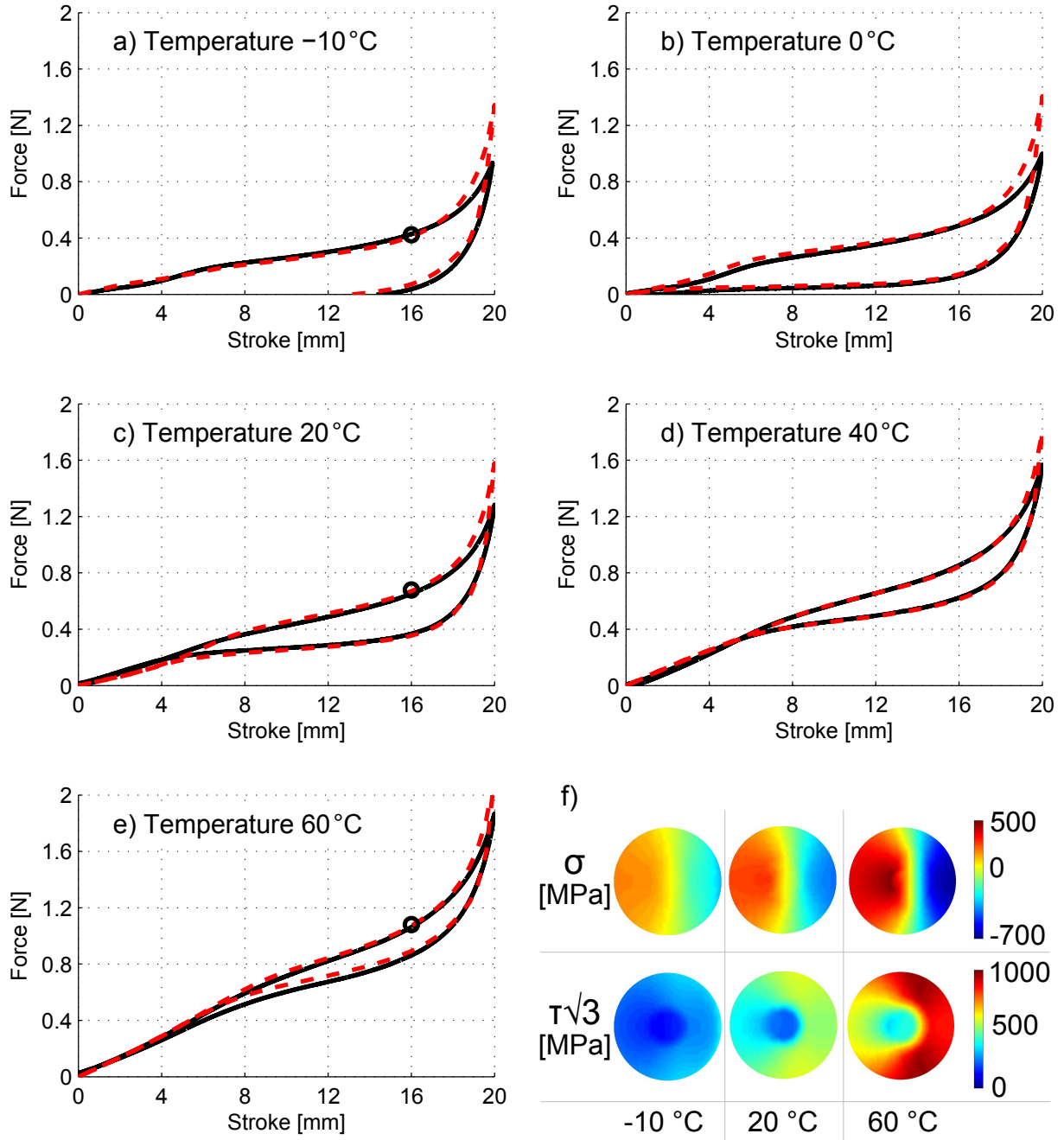
Figure 3. a)–e) Comparison of experimental (solid black line) and simulated (dashed red line) force-stroke dependence of NiTi SMA helical spring at five constant temperatures. f) Contour plots showing computed distributions of tensile/compressive stress (σ) and equivalent shear stress ($\tau\sqrt{3}$) components throughout wire cross-section at 16 mm stroke and -10, 20 and 60 °C; corresponding points denoted by black circles in a), c), e).

the wire center, the maximum of the shear stress appears in two loci which follow the shift of the tension/compression neutral axis. This results from combined effect of non-linearity of SMA response, non-proportionality of the loading, tension-compression asymmetry and strong martensite anisotropy, which imply distinct initiation and continuation of material processes at different points on wire. For instance, owing to tension-compression asymmetry, compression-induced martensite appears at higher stress and lower relative volume of the material than the tension-induced one, hence the tension/compression neutral axis is shifted (within the cross-section). It is worth noting that at 60 °C, the maximum equivalent shear stress reaches almost 1 GPa, which probably leads to local initiation of irreversible processes (e.g. plastic flow) in the material[1], even though the corresponding reduction of the spring diameter is only about 40% and the total force remains comparable to reversible cases (less than 1.2 N). This clearly shows that a guess whether and where plasticity occurs cannot be based on the value of macroscopic force alone, but local redistribution of stress must be taken into consideration. Such findings may be of practical importance for identification of a suitable working range for spring-based actuators.

5. CONCLUSIONS

In this work a macroscopic constitutive model for polycrystalline NiTi SMA exhibiting two stage martensitic transformation via R-phase, transformation strain anisotropy and tension-compression asymmetry was employed to perform numerical simulations of mechanical loading of a helical spring in a wide temperature range. Results of simulations in terms of force-stroke dependence were compared with own experimental data and discussed with respect to processes related to phase transformations occurring in the alloy. Plots of stress-components distributions at a given stroke illustrate highly non-uniform state of material across wire cross-section sensitive to temperature changes. They also allow to identify conditions and potential loci of initiation of irreversible deformation in the material.

6. ACKNOWLEDGEMENTS

References

[1] P Šittner, L Heller, J Pilch, P Sedlák, M Frost, Y Chemisky, A Duval, B Piotrowski, T Ben Zineb, E Patoor, F Auricchio, S Morganti, A Reali, G Rio, D Favier, Y Liu, E Gibeau, C Lexcellent, L Boubakar, D J Hartl, S Oehler, D C Lagoudas, and J Van Humbeeck. Roundrobin SMA modeling. In P Šittner, L Heller, and V Paidar, editors, *ESOMAT*

---

[1]This suspicion is also supported by experimental observation of residual deformation in springs loaded at temperatures above 60 °C (not presented).

2009 - The 8th European Symposium on Martensitic Transformations, page 08001. EDP Sciences, 2009.

[2] J Arghavani, F Auricchio, R Naghdabadi, A Reali, and S Sohrabpour. A 3-D phenomenological constitutive model for shape memory alloys under multiaxial loadings. *Int. J. Plast.*, 26:976–991, 2010.

[3] Y Chemisky, A Duval, E Patoor, and T Ben Zineb. Constitutive model for shape memory alloys including phase transformation, martensitic reorientation and twins accommodation. *Mech. Mater.*, 43:361–376, 2011.

[4] X Gu, W Zaki, C Morin, Z Moumni, and W Zhang. Time integration and assessment of a model for shape memory alloys considering multiaxial nonproportional loading cases. *Int. J. Solids Struct*, 54:28–99, 2015.

[5] D C Lagoudas, D J Hartl, Y Chemisky, L G Machado, and P Popov. Constitutive model for the numerical analysis of phase transformation in polycrystalline shape memory alloys. *Int. J. Plast.*, 32–33:155–183, 2012.

[6] A F Saleeb, S A Padula, and A Kumar. A multi-axial, multimechanism based constitutive model for the comprehensive representation of the evolutionary response of SMAs under general thermomechanical loading conditions. *Int. J. Plast.*, 27:655–687, 2011.

[7] A P Stebner and Brinson. Explicit finite element implementation of an improved three dimensional constitutive model for shape memory alloys. *Comput. Methods Appl. Mech. Engrg.*, 257:17–35, 2013.

[8] F Auricchio, E Bonetti, G Scalet, and F Ubertini. Theoretical and numerical modeling of shape memory alloys accounting for multiple phase transformations and martensite reorientation. *Int. J. Plast.*, 59:30–54, 2014.

[9] P Sedlák, M Frost, B. Benešová, P Šittner, and T Ben Zineb. Thermomechanical model for NiTi-based shape memory alloys including R-phase and material anisotropy under multi-axial loadings. *Int. J. Plast.*, 39:132–151, 2012.

[10] S. Stupkiewicz and H. Petryk. A robust model of pseudoelasticity in shape memory alloys. *Int. J. Numer. Meth. Engng.*, 93:747–769, 2013.

[11] F Auricchio, G Scalet, and M Urbano. A Numerical/Experimental Study of Nitinol Actuator Springs. *J. Mater. Eng. Perform.*, 23:2420–2428, 2014.

[12] M Frost, B Benešová, and P Sedlák. A microscopically motivated constitutive model for shape memory alloys: formulation, analysis and computations. *Mat. Mech. Solids*, doi: 10.1177/1081286514522474:p. not assigned yet, 2015.

[13] D J Hartl, G Chatzigeorgiou, and D C Lagoudas. Three-dimensional modeling and numerical analysis of rate-dependent irrecoverable deformation in shape memory alloys. *Int. J. Plast.*, 26:1485–1507, 2010.

[14] R Mirzaeifar, R DesRoches, and A Yavari. A combined analytical, numerical, and experimental study of shape-memory-alloy helical springs. *Int. J. Solids Struct.*, 48:611–624, 2011.

[15] L Saint-Sulpice, S Arbab Chirani, and S Calloch. Thermomechanical cyclic behavior modeling of Cu-Al-Be SMA materials and structures. *Int. J. Solids Struct.*, 49:1088–1102, 2012.

[16] A F Saleeb, B Dhakal, M S Hosseini, and S A Padula. Large scale simulation of NiTi helical spring actuators under repeated thermomechanical cycles. *Smart Mater. Struct.*, 22:094006, 2013.

[17] K Hiřmanová, J Pilch, J Racek, L Heller, P Šittner, L Recman, M Petrenec, and P Sedlák. Physical simulation of the random failure of implanted braided NiTi stents. *J. Mater. Eng. Perform.*, 23:2650–2658, 2014.

[18] G Helbert, S Saint-Sulpice, Land Arbab Chirani, L Dieng, T Lecompte, S Calloch, and P Pilvin. Experimental characterisation of three-phase NiTi wires under tension. *Mech. Mater.*, 79:85–101, 2014.

[19] J Olbricht, A Yawny, J L Pelegrina, A Dlouhý, and G Eggeler. On the stress-induced formation of R-phase in ultra-fine-grained Ni-rich NiTi shape memory alloys. *Metall. Mater. Trans. A*, 42A:2556–2574, 2011.

[20] M Frost, P Sedlák, L Kadeřávek, L Heller, and P Šittner. Mechanical response of NiTi shape memory alloy subject to combined thermal and non-proportional mechanical loading: a case study on helical spring actuator. *J. Intel. Mat. Syst. Str.*, submitted, 2015.

[21] B Reedlunn, C B Churchill, E E Nelson, J A Shaw, and S H Daly. Tension, compression, and bending of superelastic shape memory alloy tubes. *J. Mech. Phys. Solids*, 63:506–537, 2014.